

AMES REPORT IN-90

76035-CR

NUMERICAL STUDIES OF COLLAPSING INTERSTELLAR CLOUDS

P.22

NASA/Ames-University of California, Santa Cruz  
Joint Research Interchange NAG 2-368

FINAL TECHNICAL REPORT

May 1, 1987

(NASA-CR-180933) NUMERICAL STUDIES OF  
COLLAPSING INTERSTELLAR CLOUDS Final  
Technical Report (California Univ.) 25 p  
Avail: NTIS HC AC2/MF A01 CSCI 03B

N87-23340

Unclas  
G3/90 0076035

PERSONNEL

Principal Investigator: Peter Bodenheimer  
Lick Observatory  
University of California  
Santa Cruz, CA 95064

Co-investigators: Karen R. Villere  
Board of Studies in Astronomy  
and Astrophysics  
University of California  
Santa Cruz, CA 95064

David C. Black  
Space Science Division  
NASA/Ames Research Center  
Moffett Field, CA 94035

## ABSTRACT

Research conducted under this NASA/Ames-UCSC interchange has been concerned with numerical simulation of the structure and evolution of interstellar clouds. Steps have been taken toward an integrated treatment of the dynamical, thermal, and chemical processes entering model calculations, and a detailed study has been made of radiative transfer in molecular lines to allow model predictions to be tested against empirical data. It is shown that the shapes of molecular lines are sensitive to details of the cloud structure and evolutionary state and are thus useful in inferring the cloud's density, temperature, chemical composition, age, and initial conditions. The calculations have successfully reproduced and explained several observed cloud properties, including abundances of complex molecular species and the apparent depletion of CO in dense cores.

PRECEDING PAGE BLANK NOT FILMED

## I. INTRODUCTION

The objective of work performed under this NASA/Ames-UCSC research interchange has been to numerically model the structure, evolution, and observable properties of interstellar clouds in order to better understand the processes by which interstellar material is formed into stars. A large variety of physical phenomena must be considered in such a study to represent the diversity of clouds ranging from giant molecular clouds with complex structure and luminous young stars to small globules with faint infrared stars or no evidence of star formation. The research reported here has focused on the interrelated roles of dynamical, thermal, and chemical processes in time-dependent models of collapsing clouds. In particular, we have sought to understand:

- 1) The effect of the time-dependent density and temperature on chemical reaction rates and molecular composition.
- 2) The relationship between density and temperature structure and the rates of heating and cooling processes.
- 3) The influence of density, temperature, velocity, and chemical structure on molecular emission line profiles.

## II. METHOD

### a) Chemical modeling

The investigations of thermal, chemical, and radiative phenomena all utilize detailed and self-consistent numerical models for the dynamical evolution of gas clouds subject to forces of gravity and internal pressure. A hydrodynamic code provides time dependent models of internal structure for clouds evolving from initially uniform and quiescent states to configurations with large gradients of velocity, density and temperature. The chemical studies have used spherical collapse models calculated with the code of Bodenheimer 1968. (This one-dimensional treatment neglects effects of rotation and magnetic fields.) The only major modification to this code has been the in treatment of the gas kinetic temperature--the principal link between dynamics and chemistry. The temperature has been prescribed as a function of density and optical depth by the semi-empirical formula of Tarafdar, Prasad, Huntress, Villere, and Black 1985, which contains the essential physics of heating and cooling processes and is in agreement with temperatures measured in both diffuse and dense clouds. The density and temperature from the hydrodynamic calculations is used with the evolutionary chemistry code of Prasad and Huntress 1980, which for the present study has been extended to include 180 chemical and molecular species and 1626 reactions. The resulting molecular concentrations and column densities are compared with cloud observations in Section III.

### b) Thermal structure

A major step toward a fully consistent treatment of dynamical and thermal processes was undertaken with the cooperation of Dr. S. Tarafdar of the Tata Institute for Fundamental Research, Bombay. A code was developed to follow the dynamical evolution of spherically symmetric clouds in which temperature is determined through heating by interstellar UV radiation, cosmic rays, molecule formation, and

gravitational compression and cooling by molecular line emission and grain thermal emission. Because this code does not yet contain detailed molecular chemistry, initial applications were restricted to the early phases of cloud collapse.

### c) Molecular lines

Emission line profiles of CO isotopes have been calculated for both rotating and nonrotating clouds modeled with the 2D hydrodynamic code of Black and Bodenheimer 1975. This code also has been modified to include the temperature parameterization of Tarafdar et al., and the nonrotating models are consistent with models obtained with the 1D code. For the dynamical calculations the gas composition is entirely  $H_2$ , but a small admixture of CO isotopes is assumed for the emission profiles. Spatially uniform abundances of  $^{12}CO$ ,  $^{13}CO$ , and  $C^{18}O$  are used, except that at small optical depth ( $\tau_{vis} \approx 2$ ) the abundance of each isotope is decreased in proportion to  $\tau_{vis}$ , and for  $\tau_{vis} \leq 4$ ,  $^{12}CO \rightarrow ^{13}CO$  fractionation is modeled after results by Langer 1977. In some models the CO abundances have been reduced at high density ( $n(H_2) > 10$ ) in accordance with the observations and interpretation of Wootten et al. 1978 and 1980.

A numerical code has been developed to solve the coupled equations of statistical equilibrium and radiative transfer for CO rotational lines. In the calculation of level populations, the radiative intensity is obtained from the local density, temperature, and velocity by the Sobolev formalism (Sobolev 1960), and collisional excitation rates are taken from Green and Thaddeus 1976. With the populations and source function thus determined, emission line profiles are obtained by integrating the transfer equation for selected frequencies and lines of sight. The line shape function for these integrations is that of Doppler broadening at the local kinetic temperature. This procedure is an improvement over the standard technique of local approximation for both the source function and line intensity, allowing in at least a first approximation for effects of large or nonmonotonic gradients in temperature, density and velocity.

## III. RESULTS

### a) Chemical modeling

Several numerical experiments were conducted to extend the work of Tarafdar et al. and to address the questions of: i) large C abundances observed in dense clouds ( $N(CI)/n(CO)$  between 0.01 and 0.1); ii) the non-detection of  $O_2$  in dense clouds; and iii) failure of previous chemistry studies, notably those employing hydrostatic models, to reproduce both the C abundance and abundances of complex H-C-O molecules.

Some investigators have suggested a C/O abundance ratio greater than one to explain the large C abundance, but this leads to overabundance of other carbon compounds (ie.  $C_2H$ ,  $C_3H$ ,  $C_3H_2$ ). In the present models the abundance of C relative to CO has been enhanced in the cloud interior through dissociation of CO by UV radiation from cosmic ray excitation of the Lyman and Werner bands of  $H_2$ . The formation of  $O_2$  has been suppressed by reducing the rate of  $O + OH \rightarrow O_2 + H$  on the basis of recent experimental data and by channeling O into  $H_2O$  through the assumption that  $H_2O$  is the primary product of  $H_3O^+$  recombinations. The non-detection of  $H_2O$  in most dark clouds can be explained if this molecule is frozen onto grains.

Calculations with the above assumptions have been successful in reproducing observed abundances of O, O<sub>2</sub>, H<sub>2</sub>O, CO, and C<sub>2</sub>H, but the predicted abundances of C<sub>3</sub>H, and C<sub>3</sub>H<sub>2</sub> are too small. It is found, however, that hydrocarbon abundances may be enhanced by artificially slowing the collapse rate (evolutionary time steps increased by a factor of 10). This suggests that non-gravitational forces (rotation, turbulence, and/or magnetic fields) may play an important role in both the dynamical and chemical evolution. Additional experiments have shown that increasing the temperature in high density cloud cores to 20-50 K (as compared with ~10 K obtained from the Tarafdar et al. formula) gives better abundances of several complex species, including CH<sub>3</sub>OH, CH<sub>3</sub>CN, and CH<sub>3</sub>COH. This result implies that additional heating sources, such as newly formed stars or protostars, may be present although not always detected.

#### b) Thermal structure

Two projects were undertaken with the integrated hydrodynamic and thermodynamic code. The first calculations concentrated on comparison of the temperature derived from detailed heating and cooling models with the semi-empirical temperature of Tarafdar et al. The code includes two numerical coefficients specifying the efficiency of grain photoelectron heating and the depletion of heavy elements, which may be varied within limits of experimental and observational uncertainty. For coefficient values within the permitted range, it is found that the dependence of temperature on density and optical depth is in good agreement with predictions of the semi-empirical formula.

Additional calculations performed to determine the minimum mass for gravitational collapse as a function of cloud density showed that this critical mass can be an order of magnitude smaller than the Jeans mass for isothermal clouds. These results are qualitatively consistent with predictions for the stability of gas spheres with polytropic temperature variation (Viala and Horedt 1974), but the critical mass values differ because the temperature is not polytropic when heating and cooling processes are treated in detail.

#### c) Molecular lines

Time sequences of models used in the calculation of CO lines were generated as functions of three parameters: the cloud mass, initial density, and initial rotational velocity. Although the details of the evolution depend on values given to these parameters, the sequences show qualitative similarities that are reflected in general features of the spectral line shapes. The nonhomologous collapse produces a steep, centrally-peaked density profile. In rotating models, collapse is most rapid in the direction of the rotation axis, and the mass distribution becomes increasingly flattened. Eventually centripetal effects reverse the collapse near the cloud center, producing an off-center density maximum (a "ring") in the equatorial plane (cf. Black and Bodenheimer 1976). Both the collapse and rotational velocities are nonmonotonic, increasing with radius near the cloud center but decreasing in the outer layers. The gas temperature increases with radius because of decreasing density and optical depth.

An example of cloud structure and line profile calculations is given in Figures 1 through 4, which illustrate the evolution of a 100 M<sub>⊙</sub> cloud from an initial state of density 40 cm<sup>-3</sup> and angular velocity 5 x 10<sup>-15</sup> s<sup>-1</sup>. Profiles are shown for models at which the maximum density in the cloud is 10<sup>3</sup>, 10<sup>4</sup>, and 10<sup>5</sup> cm<sup>-3</sup>. For each model the J = 1→0 brightness temperature of the three commonly observed CO isotopes is shown as a function of velocity for lines of sight at the indicated offsets x = R/R<sub>max</sub> from the cloud center. In Figures 1

through 3 the lines of sight are in the equatorial plane, and in Figure 4 they are in the direction of the rotation axis. Also shown for each model is the variation in the equatorial plane of density, collapse and rotational velocities, kinetic temperature ( $T_k$ ), excitation temperature ( $T_x$ ), and CO isotope abundances.

Several features of the line profiles give evidence of the form of density, temperature, and velocity distributions and of the time since initiation of collapse. The characteristic flattening and turnover of the velocity profile in these models produces a minimum in line intensity because low excitation foreground material obscures warmer material of the same velocity. That this minimum occurs at positive velocity is evidence that the cloud is collapsing rather than expanding. Rotational motion shifts the centroid of the line profile toward higher velocity with increasing offset  $x$ . (At positive  $x$  the direction of rotation is away from the observer.) Rotation also produces the differing line shapes at positive and negative  $x$ . The effects of rotation are absent in Figure 4 where the view is along the rotation axis. In the later models, the combination of outwardly increasing kinetic temperature and outwardly decreasing density produces maximum excitation temperature away from the cloud center. This leads to the off-center maxima in line intensity seen in Figures 2 and 3. The presence of two maxima in excitation temperature along a line of sight through the cloud center gives rise to the double emission peak in Figure 2. Finally, the relative intensities of the CO isotopes are seen to be sensitive indicators of cloud density and evolutionary state. At the cloud center, the line intensity of  $^{12}\text{CO}$  decreases as increasing density and optical depth lower the kinetic and excitation temperatures. The intensity of the unsaturated  $\text{C}^{18}\text{O}$  line increases with time as increasing density brings  $T_x$  closer to  $T_k$ . The intensity of  $^{13}\text{CO}$  shows both effects, increasing at first and then decreasing.

For clouds models of larger mass, the line profiles are broader than those of Figure 4. The larger optical depth of these clouds results in lower temperature and pressure and larger collapse velocity and also in increased saturation of the high velocity line wings. (See figures 5 and 6 for profiles in a cloud with mass  $1000 M_\odot$ .) A similar effect results from the assumption of larger initial cloud density. (Compare Figure 5 for a cloud with  $n_0 = 40 \text{ cm}^{-3}$  and Figure 6 for a cloud with  $n_0 = 4 \text{ cm}^{-3}$ .) If the initial rotation rate is reduced, the line shapes approach those of the rotating cloud viewed pole-on. (See Figure 7 for a nonrotating cloud.)

Because the comparison of theoretical and observed line profiles is essential both for refining physical input to the models and for meaningful interpretation of empirical data, effort has been made to present the theoretical results in forms suitable for direct comparison with observations. The lightly drawn curves in Figure 3 are profiles that would be observed if the model cloud was placed at a distance of 400 pc and observed with a "state-of-the-art" telescope having a gaussian antenna profile of FWHM = 1' and filters of width 0.1 km/sec. Because in this case the beam is much smaller than the cloud diameter (22') and the filter width is smaller than the width of principal line features, the line shapes are not qualitatively altered. For clouds of smaller size, the effects of beam smoothing will be more severe.

Effects from the addition of a microturbulent component to the line broadening have also been investigated, although the results have only qualitative significance because the Sobolov approximation for the excitation temperature becomes less accurate. Line shapes are little changed unless the turbulent velocity is of the order of the macroscopic fluid velocity. Figure 5 shows the profiles of Figure 2 with the addition of spatially uniform turbulence with characteristic velocity 0.5 km/s. With turbulence the profiles are wider and more rounded, and only the  $^{12}\text{CO}$  lines have double peaks.

Unfortunately observers rarely publish line profiles mapped across a cloud, the data most useful for comparison with numerical models. For this reason the present theoretical results have also been expressed in a form more commonly seen in the literature: mappings of maximum line brightness, line width, and line centroid velocity. Examples of these mappings are shown in Figures 6 for the cloud model corresponding to Figure 1.

The theoretical line profiles were also used to assess the accuracy of commonly used methods by which physical parameters are deduced from observed profiles and simplified cloud models. Particularly noteworthy are results pertaining to the abundance ratio  $n(^{13}\text{CO})/n(\text{H}_2)$ . Several investigators (eg. Wootten et al. 1978 and 1980) find that the relative  $^{13}\text{CO}$  abundance decreases sharply with increasing total gas (or  $\text{H}_2$ ) density and suggest that CO freezes onto dust grains. The present work has shown that this apparent relationship between CO density and total density can result from an improper comparison of observational data: the lines used to derive the total gas density ( $\text{H}_2$ , CO and other molecules of high excitation energy) are formed near the cloud center, whereas CO lines are formed in the outer cloud. The "observed" abundance variation can be reproduced using  $n(^{13}\text{CO})$  at the depth where the  $^{13}\text{CO}$  line is formed ( $\tau_{13} = 1$ ) and  $n(\text{H}_2)$  at the cloud center, but if both densities refer to  $\tau_{13} = 1$  the ratio  $n(^{13}\text{CO})/n(\text{H}_2)$  shows little variation with  $n(\text{H}_2)$ . (See example in Figure 7.) It is thus reasonable to suspect large errors in many published molecular abundances and column densities.

#### IV. SUMMARY AND CONCLUSIONS

Significant steps have been taken toward a comprehensive and integrated numerical treatment of dynamical, thermal, and chemical phenomena in interstellar clouds and toward the use of molecular line profiles for meaningful comparison of cloud models and observational data. Chemical evolution has been studied in the context of detailed hydrodynamical models, and, likewise, the thermodynamic processes that influence cloud temperature and reaction rates have been related to chemical and dynamical properties. Moreover, detailed treatment of line radiative transfer has shown that CO profiles are sensitive to cloud structure and evolutionary state, thus opening opportunities for their use in discriminating among alternative theoretical models and in deriving cloud parameters not easily inferred from observation alone. In particular the line shapes are shown to reveal information on the cloud's density, temperature, velocity, chemical composition, mass, and age. It must be realized, however, that in spite of these advances, further work is still needed for a fully consistent and complete understanding of the physical properties and evolution of interstellar clouds.

## REFERENCES

- Black, D.C., and Bodenheimer, P. 1975, Ap. J., 199, 619.  
\_\_\_\_\_. 1976, Ap. J., 206, 138.
- Bodenheimer, P. 1968, Ap. J., 153, 683.
- Green, S., and Thaddeus, P. 1976, Ap. J., 205, 766.
- Langer, W.D. 1977, Ap. J. (Letters), 212, L39.
- Snell, R.L. 1979, Ph.D. thesis, University of Texas.
- Prasad, S.S., and Huntress, W.T. 1980, Ap. J. Suppl., 43, 1.
- Sobolev, V.V. 1960, Moving Envelopes of Stars (Cambridge: Harvard Univ. Press).
- Tarafdar, S.P., Prasad, S.S., Huntress, W.T., Villere, K.R., and Black, D.C. 1985, Ap. J., 289, 220.
- Viala, Y.P., and Horedt, G. 1974, Astron. Astrophys., 33, 195.
- Wootten, A., Evans, N.J., Snell, R., and Vanden Bout, P. 1978, Ap. J. (Letters), 225, L143.
- Wootten, A., Snell, R., and Evans, N.J., Ap. J. 1980, 240, 532.

## FIGURES

Figures 1, 2, 3, and 4 refer to models for a cloud with mass  $100 M_{\odot}$  and initial density  $n_0 = 40 \text{ cm}^{-3}$ .

Fig. 1a - Emission profiles of the  $J = 1 \rightarrow 0$  rotational transitions of  $^{12}\text{CO}$ ,  $^{13}\text{CO}$ , and  $\text{C}^{18}\text{O}$  for the evolutionary model with maximum density  $n = 10^3 \text{ cm}^{-3}$ , maximum visual extinction  $A_V = 3$ , and age  $t = 3.4 \times 10^6 \text{ yr}$ . Brightness temperature is shown as a function of velocity for lines of sight in the equatorial plane at the indicated offsets  $x = R/R_{\text{MAX}}$  from the cloud center.

Fig. 1b - Variation with  $R$  in the equatorial plane of density, collapse and rotational velocities, kinetic temperature, excitation temperature, and CO isotope abundances for the model with maximum density  $n = 10^3 \text{ cm}^{-3}$ .

Fig. 2a - CO emission profiles for the model with maximum density  $n = 10^4 \text{ cm}^{-3}$ , maximum visual extinction  $A_V = 14$ , and age  $4.4 \times 10^6 \text{ yr}$ .

Fig. 2b - Variation with  $R$  in the equatorial plane of density, collapse and rotational velocities, kinetic temperature, excitation temperature, and CO isotope abundances for the model with maximum density  $n = 10^5 \text{ cm}^{-3}$ .

Fig. 3a - CO emission profiles for the model with maximum density  $n = 10^5 \text{ cm}^{-3}$ , maximum visual extinction  $A_V = 70$ , and age  $4.8 \times 10^6 \text{ yr}$ .

Fig. 3b - Variation with  $R$  in the equatorial plane of density, collapse and rotational velocities, kinetic temperature, excitation temperature, and CO isotope abundances for the model with maximum density  $n = 10^5 \text{ cm}^{-3}$ .

Fig. 4a - CO emission profiles for the model with maximum density  $n = 10^4 \text{ cm}^{-3}$ , viewed in the direction perpendicular to the equatorial plane.

Fig. 4b - Variation with  $Z$  along the symmetry axis of density, collapse and rotational velocities, kinetic temperature, excitation temperature, and CO isotope abundances for the model with maximum density  $n = 10^4 \text{ cm}^{-3}$ .

Fig. 5 - CO emission profiles of a cloud with mass  $1000M_{\odot}$  and initial density  $n_0 = 40 \text{ cm}^{-3}$  for the model with maximum density  $n = 10^4 \text{ cm}^{-3}$ .

Fig. 6 - CO emission profiles of a cloud with mass  $1000M_{\odot}$  and initial density  $n_0 = 4 \text{ cm}^{-3}$  for the model with maximum density  $n = 10^4 \text{ cm}^{-3}$ .

Fig. 7 - CO emission profiles of a nonrotating cloud with mass  $100 M_{\odot}$  and initial density  $n_0 = 40 \text{ cm}^{-3}$  for the model with maximum density  $n = 10^4 \text{ cm}^{-3}$ .

Fig. 8 - CO emission profiles for the model with maximum density  $n = 10^4 \text{ cm}^{-3}$ , with the addition of uniform turbulence of characteristic velocity  $0.5 \text{ km/s}$ .

Fig. 9a, 9b, 9c - Contours of  $^{13}\text{CO}$  brightness temperature, line width (FWHM), and line velocity for the model with maximum density  $n = 10^3 \text{ cm}^{-3}$ .

Fig. 10 - Abundance ratio  $n(^{13}\text{CO})/n(\text{H}_2)$  observed in a variety of interstellar clouds and derived from models shown in Figures 1-4. The filled circles are measurements by Wootten et al. 1978; open circles are measurements by Snell 1979. The values labeled X are derived from the model profiles by the method of Wootten and Snell, and values labeled + are from actual model abundances at  $\tau_{13} = 1$ .

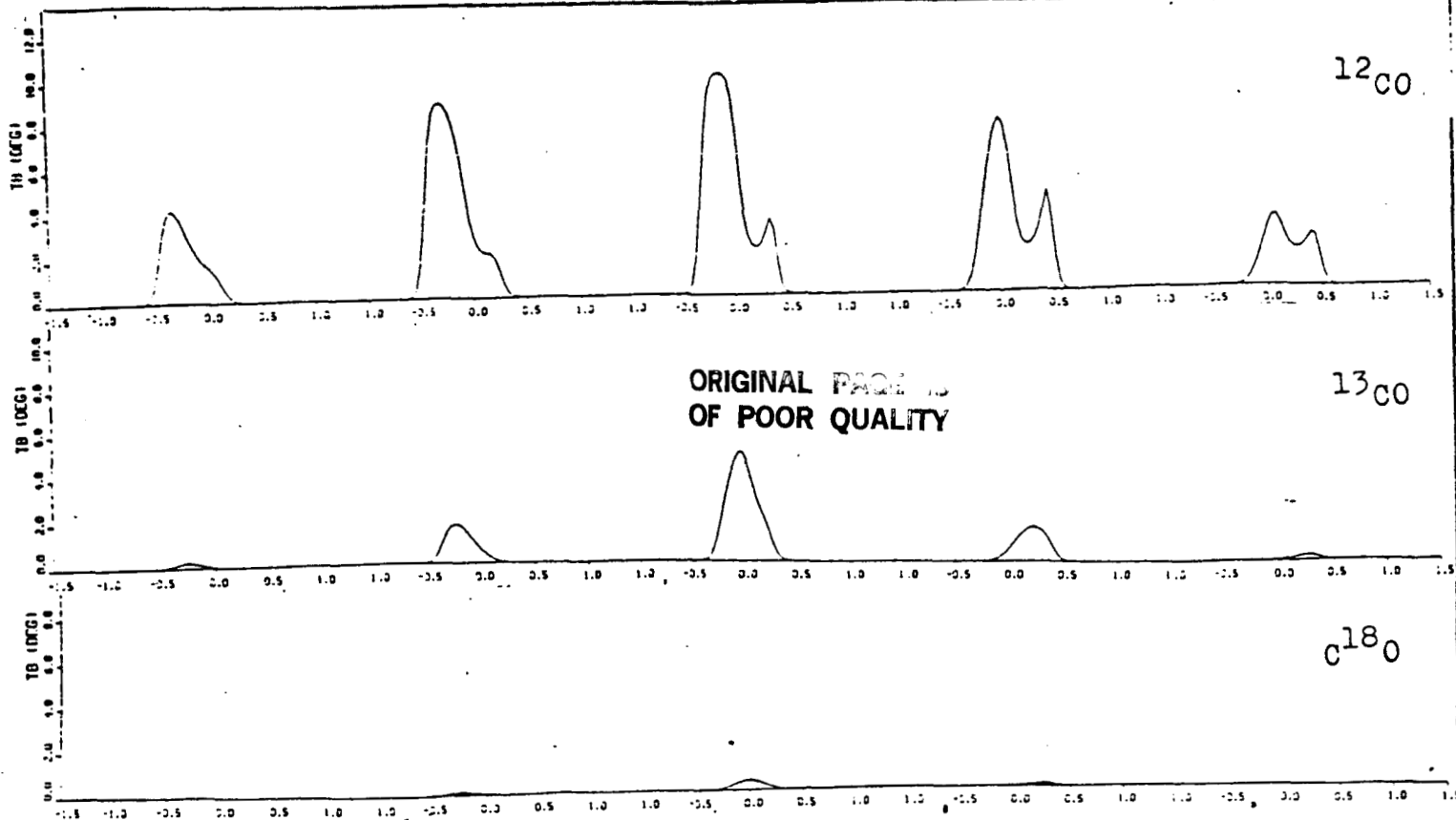


Fig. 1a

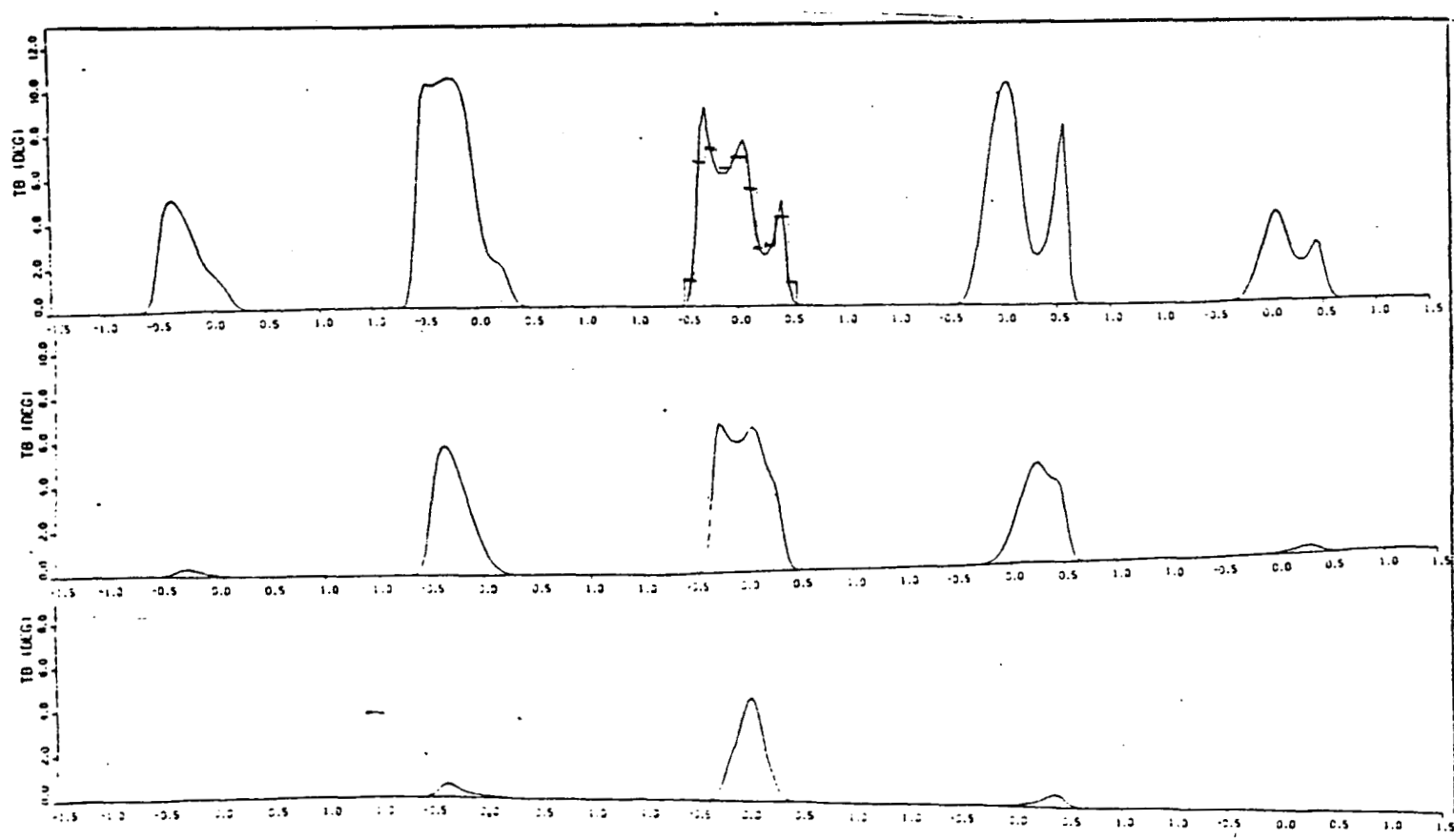


Fig. 2a

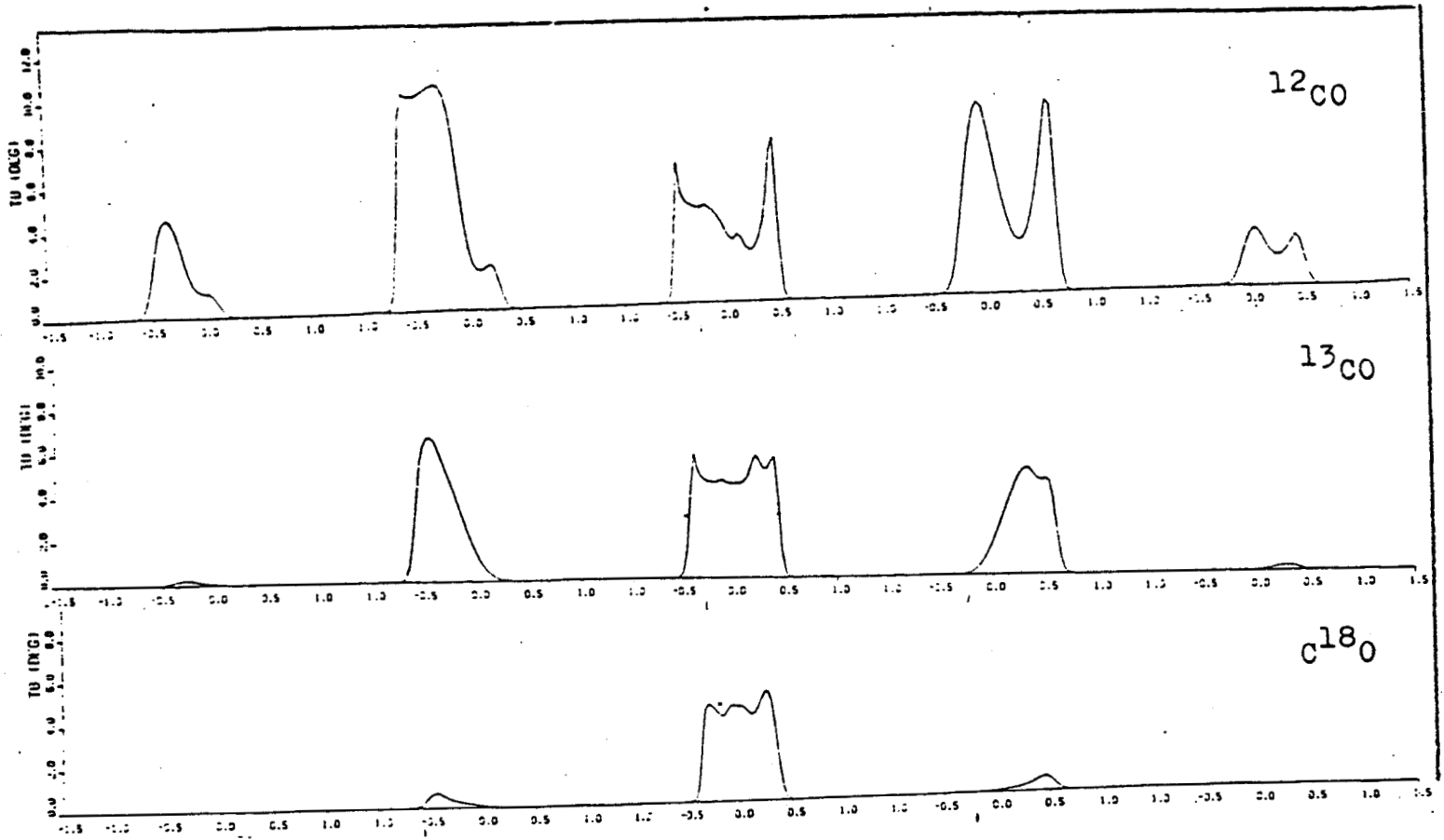
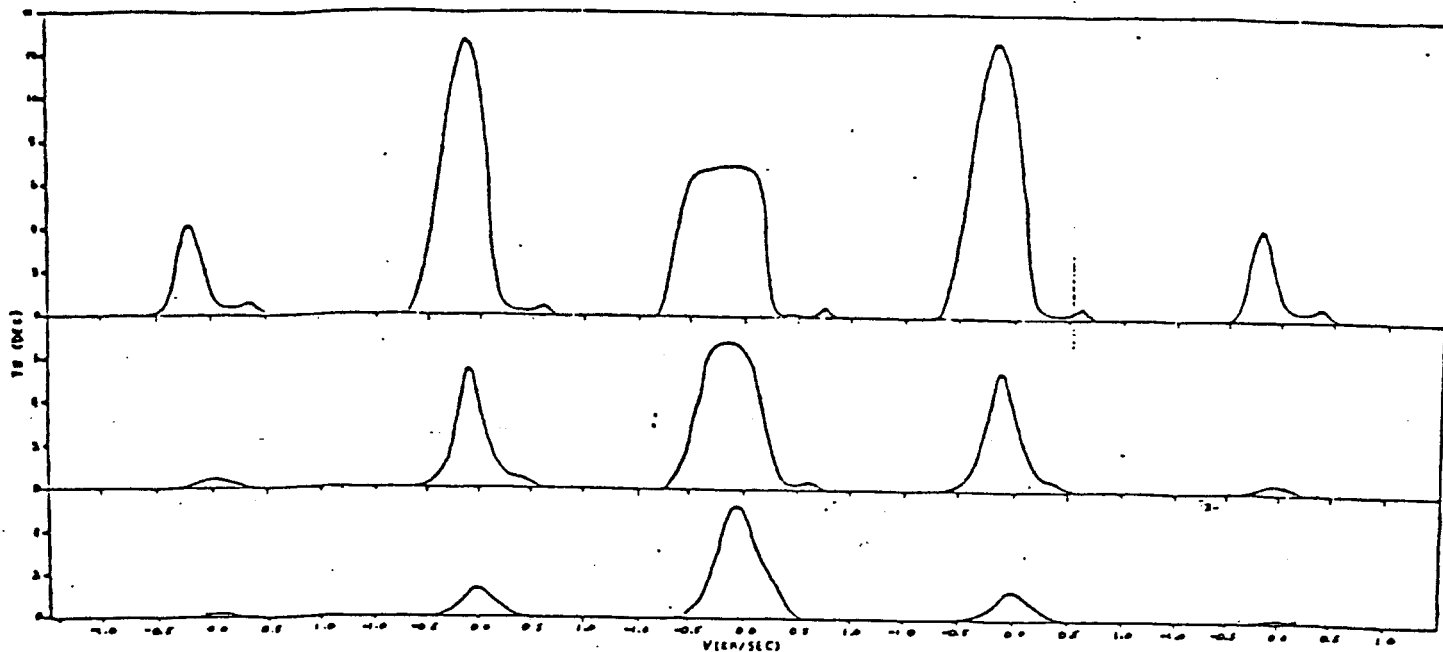


Fig. 3a

ORIGINAL PAGE IS  
OF POOR QUALITY

fig. 4a



ORIGINAL PAGE IS  
OF POOR QUALITY

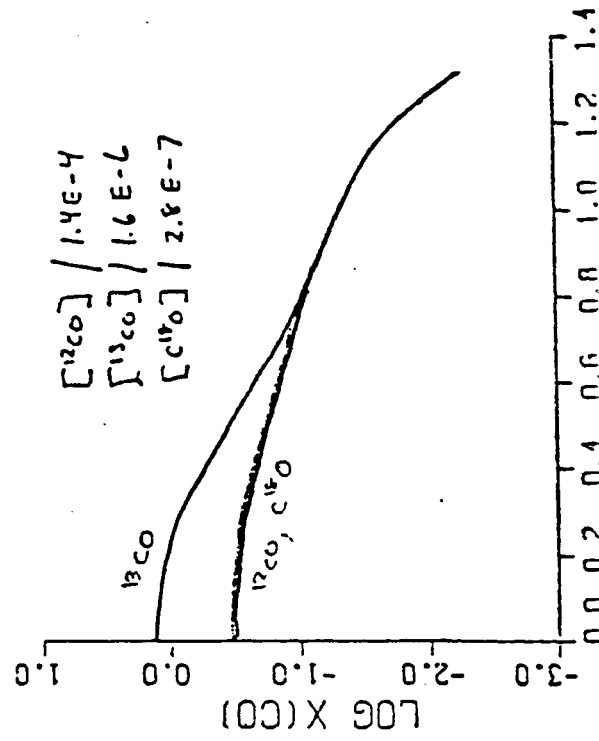
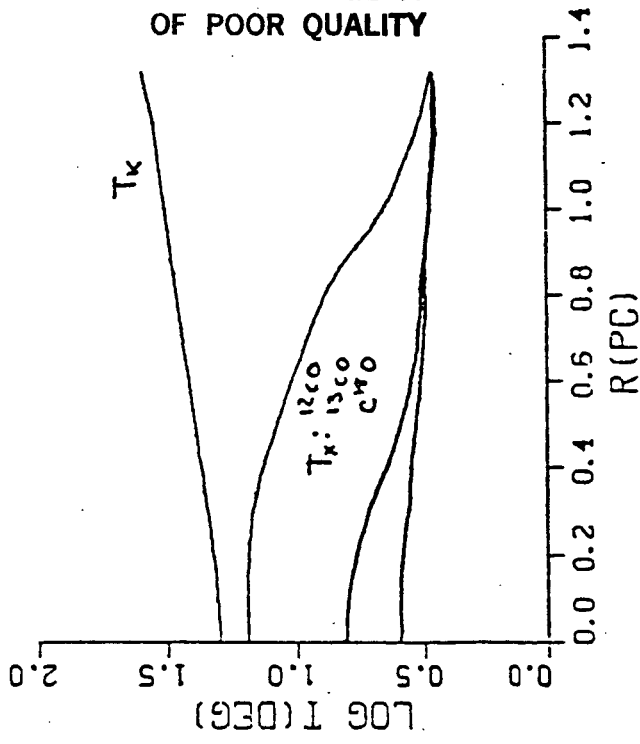


Figure 1b

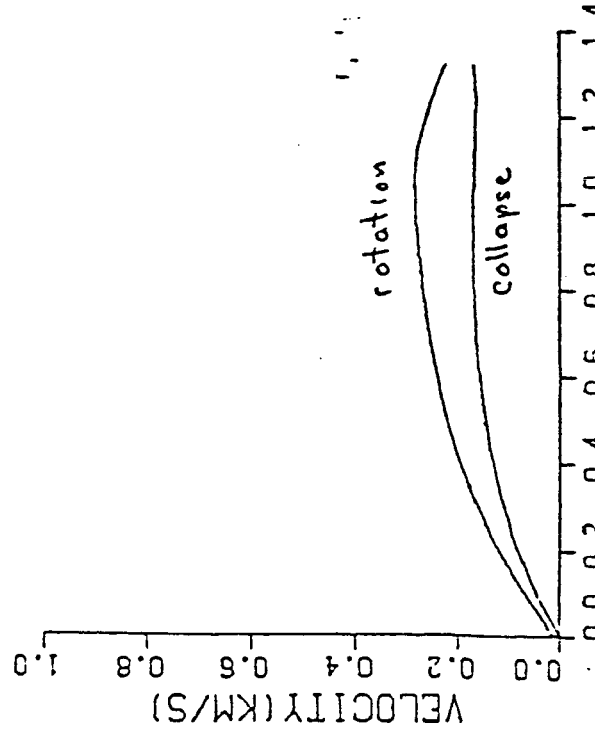
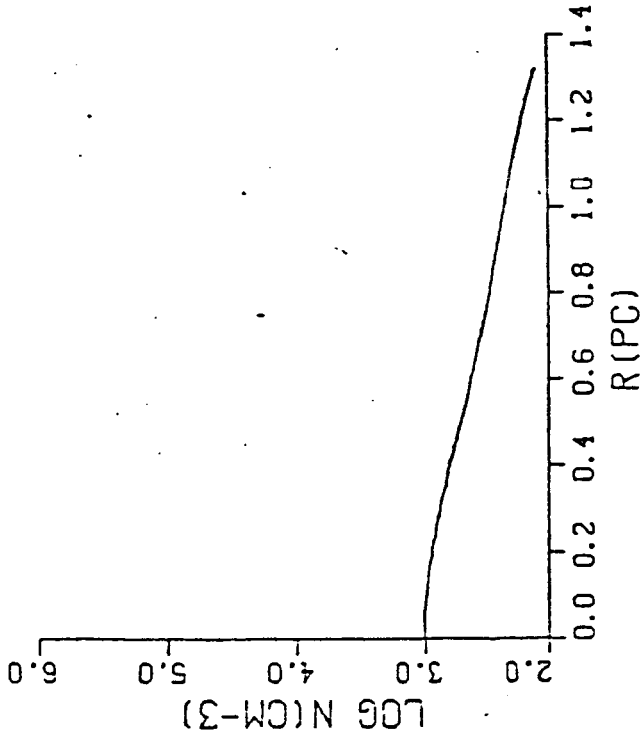


Figure 2b

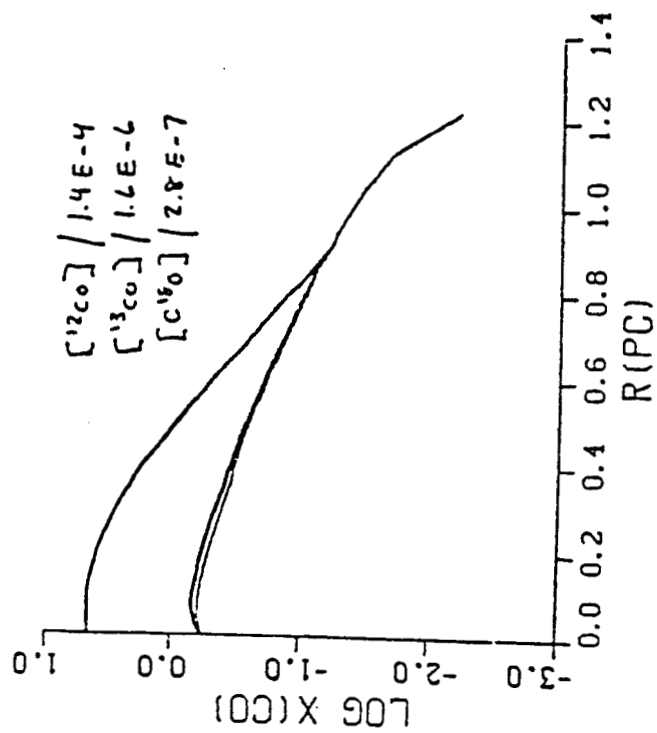
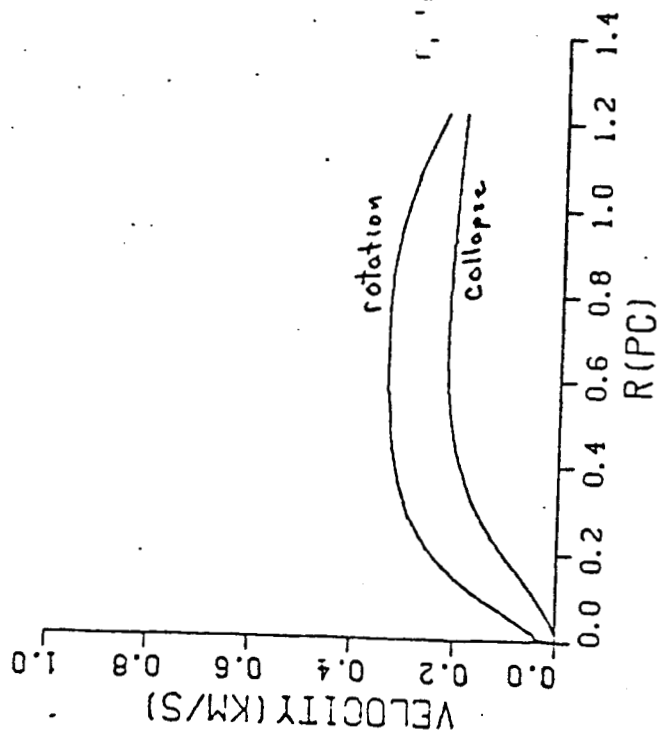
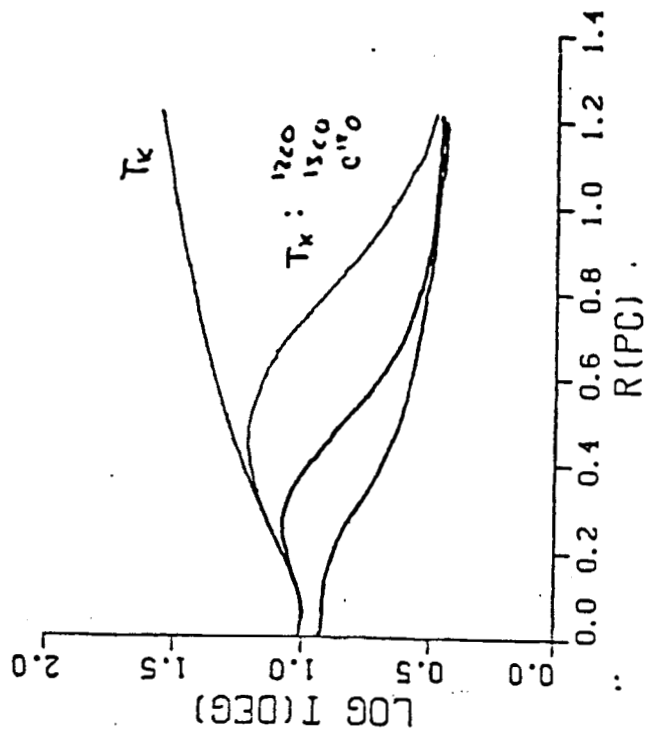
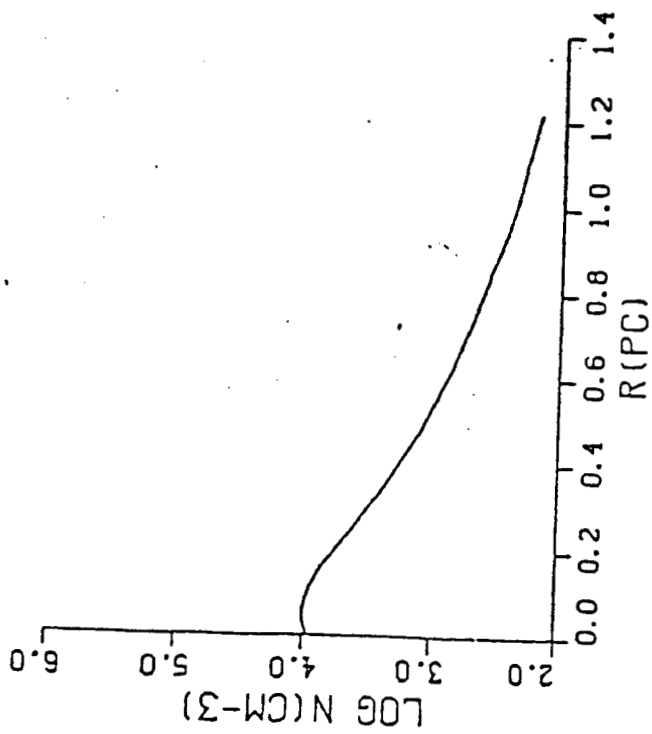
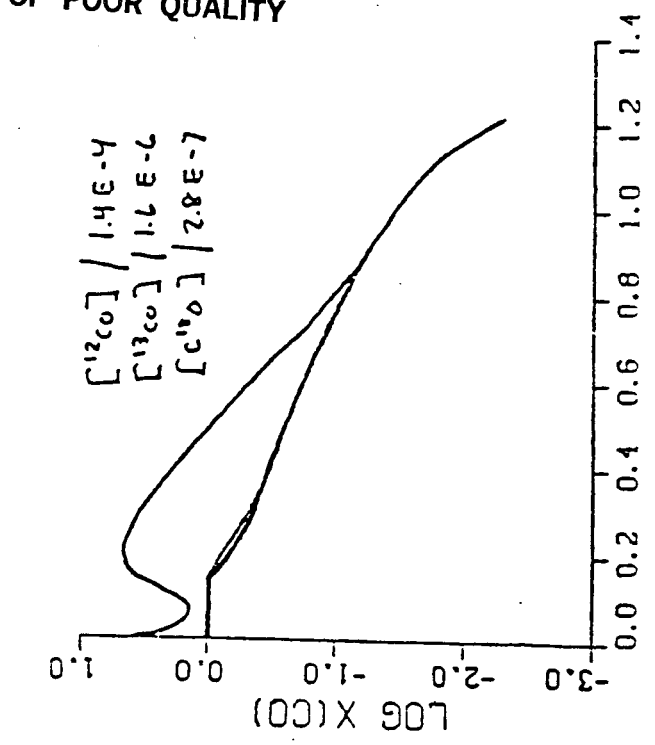
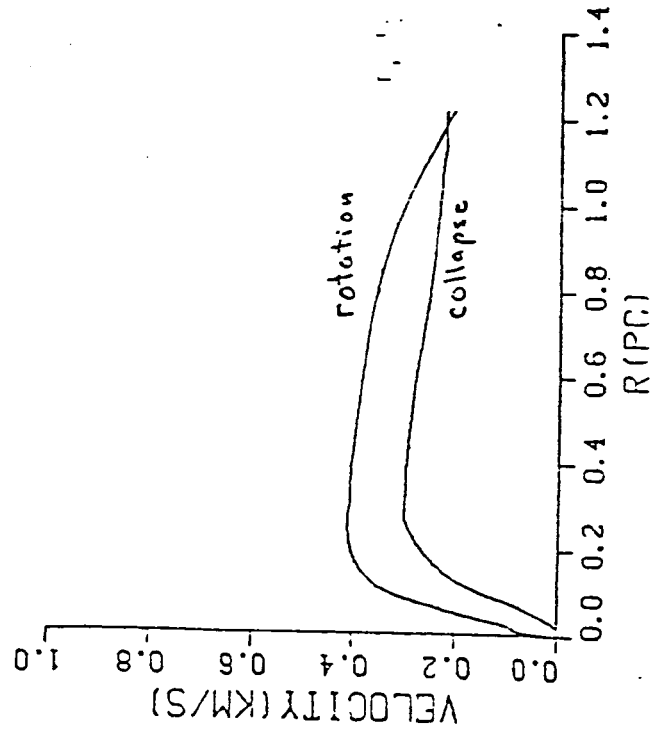
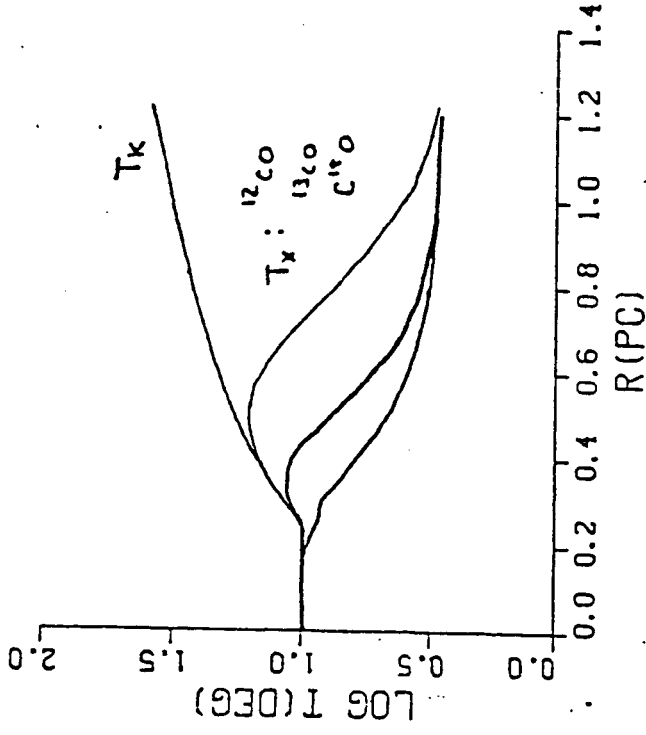
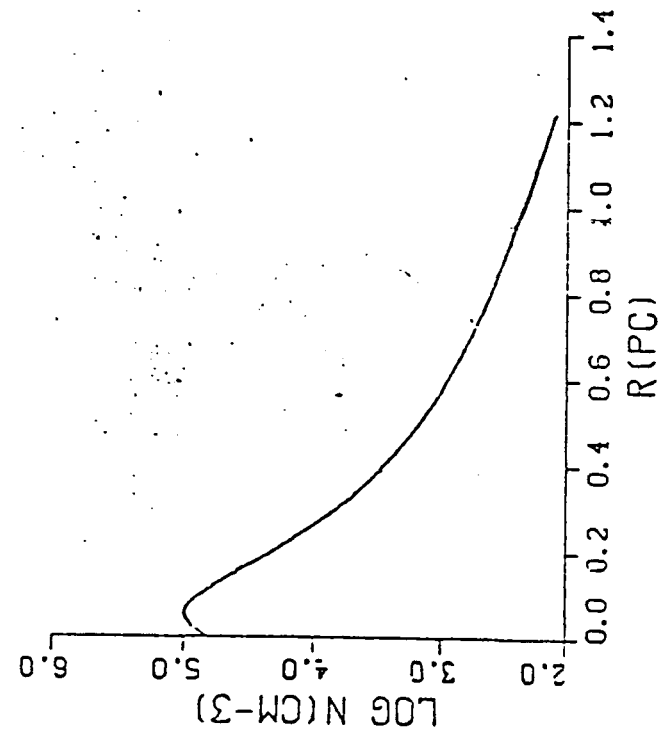
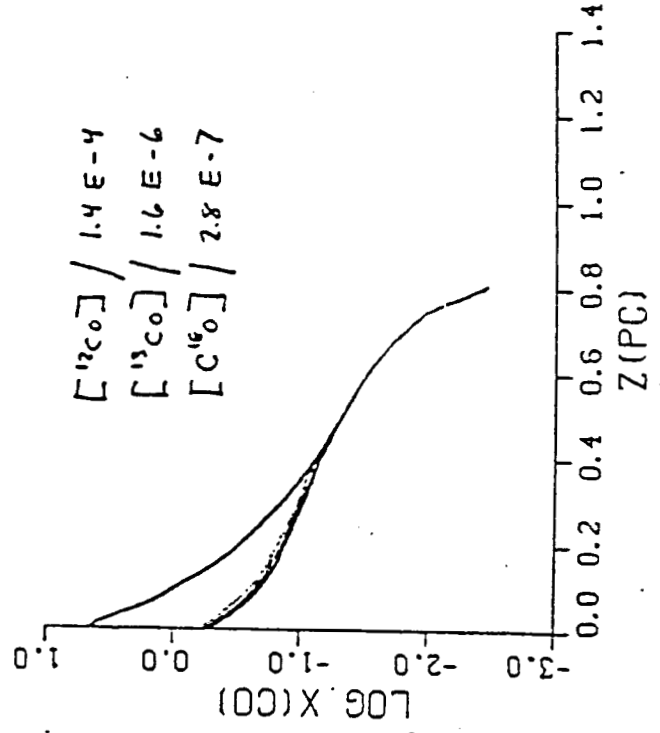
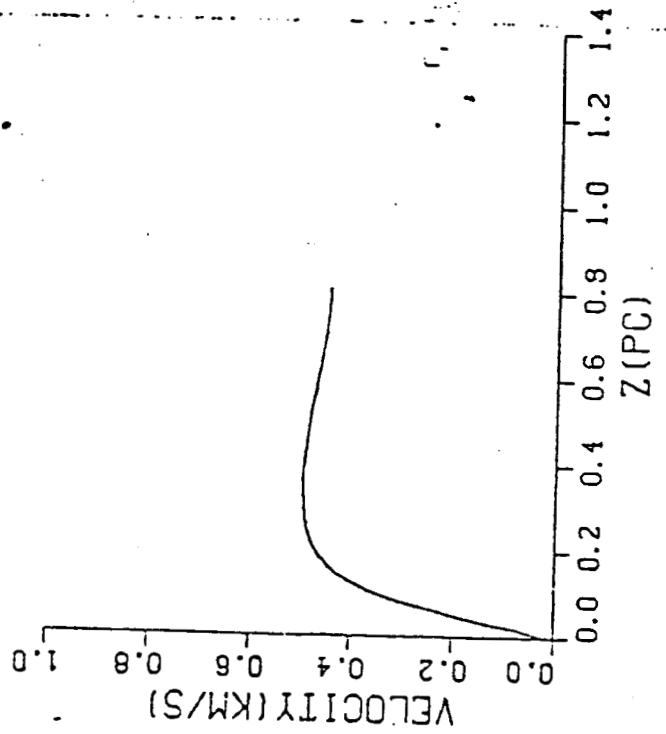
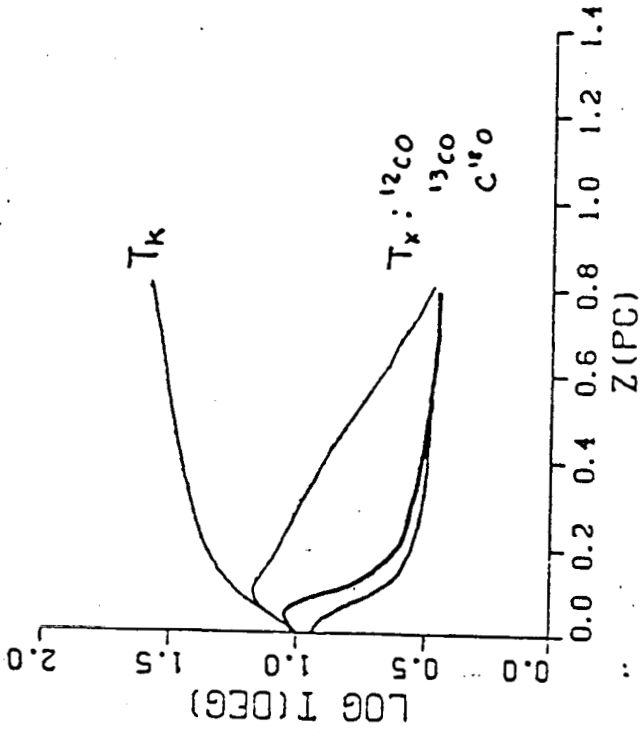
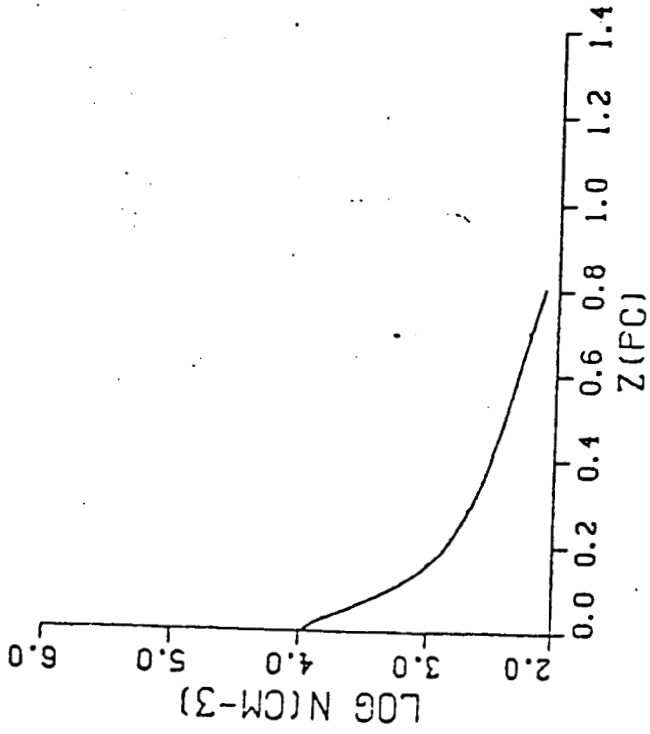


Figure 3b



ORIGINAL PAGE IS  
OF POOR QUALITY

Figure 4b



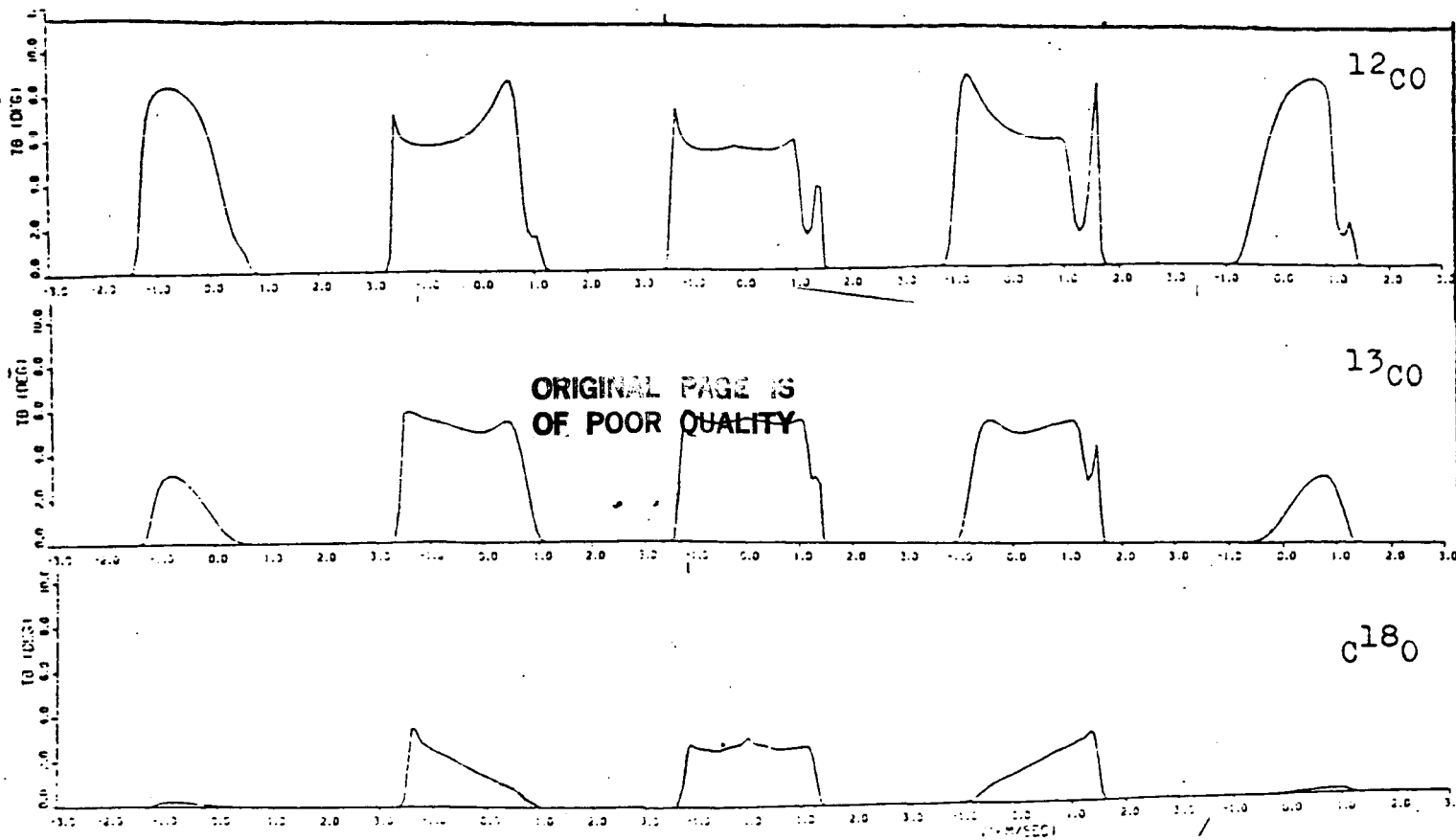


Fig. 5

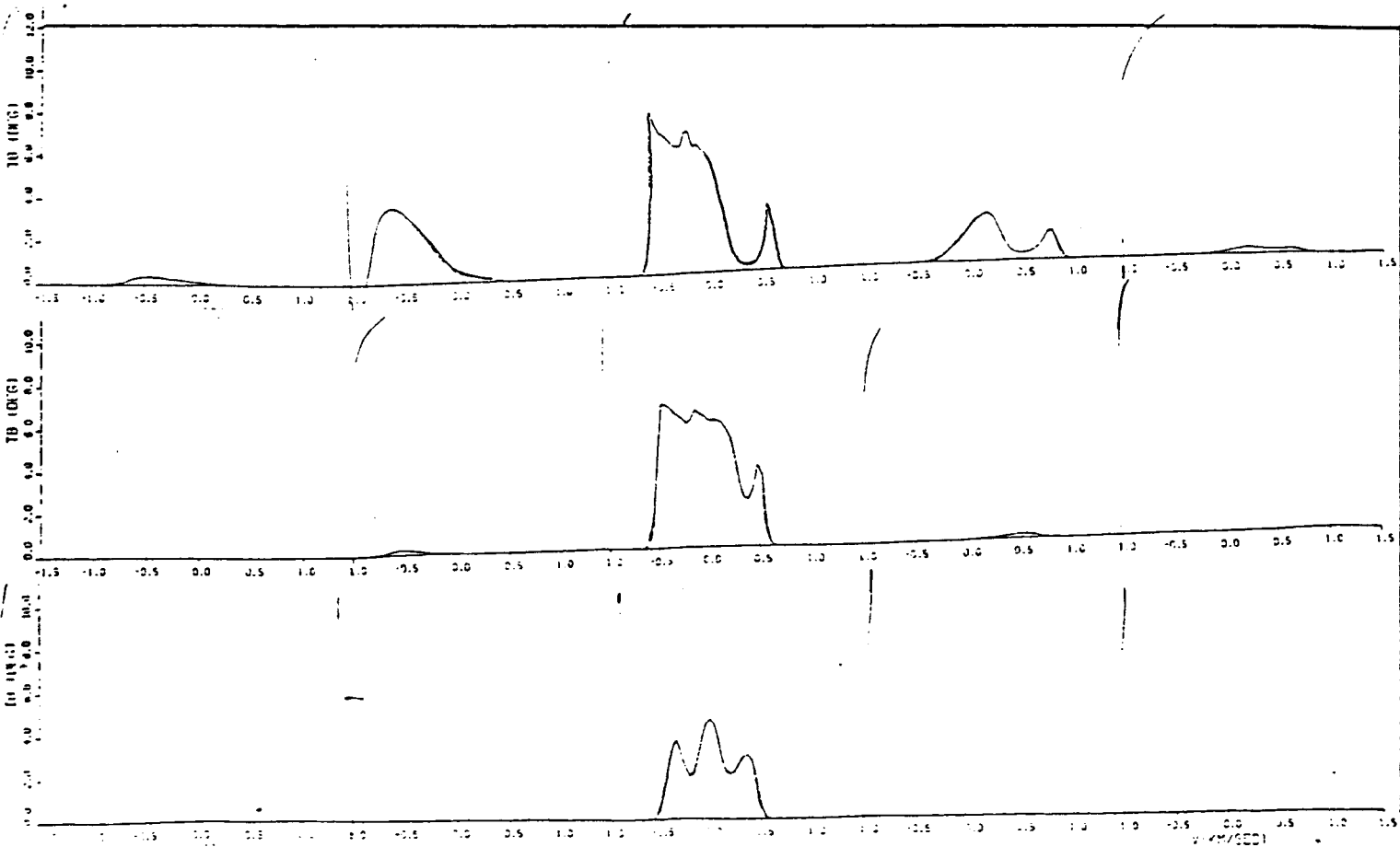


Fig. 6

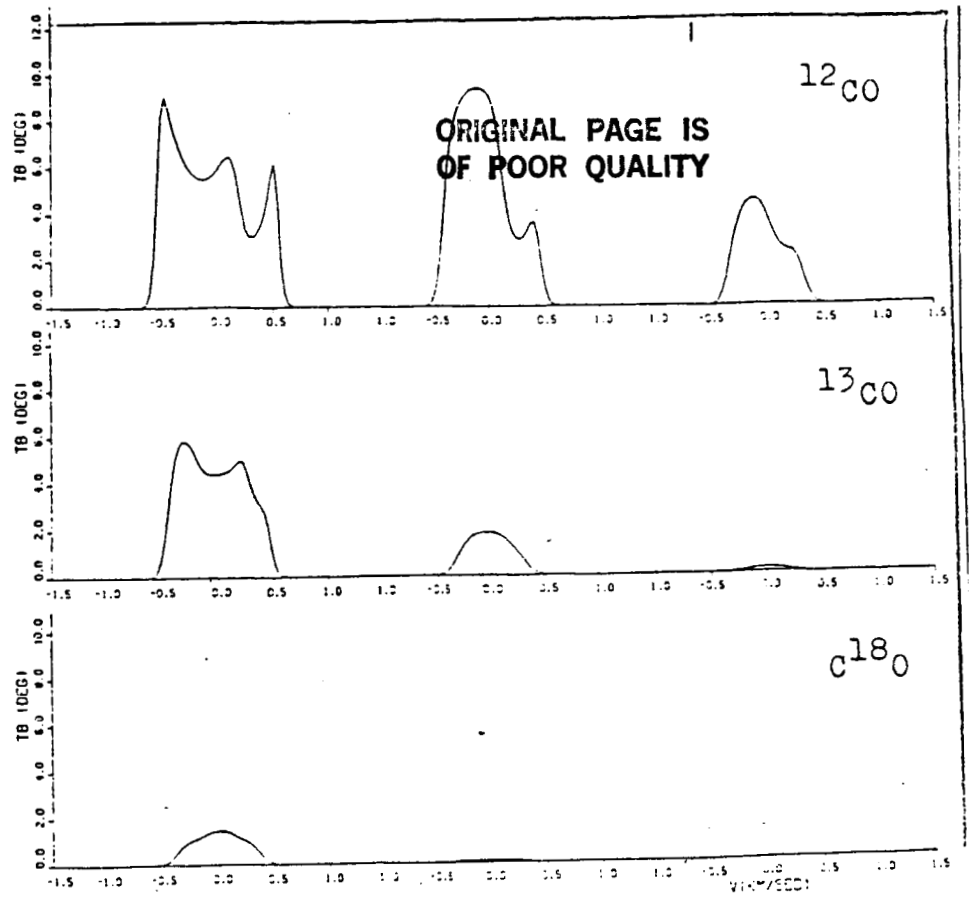


Fig. 7

ORIGINAL PAGE IS  
OF POOR QUALITY

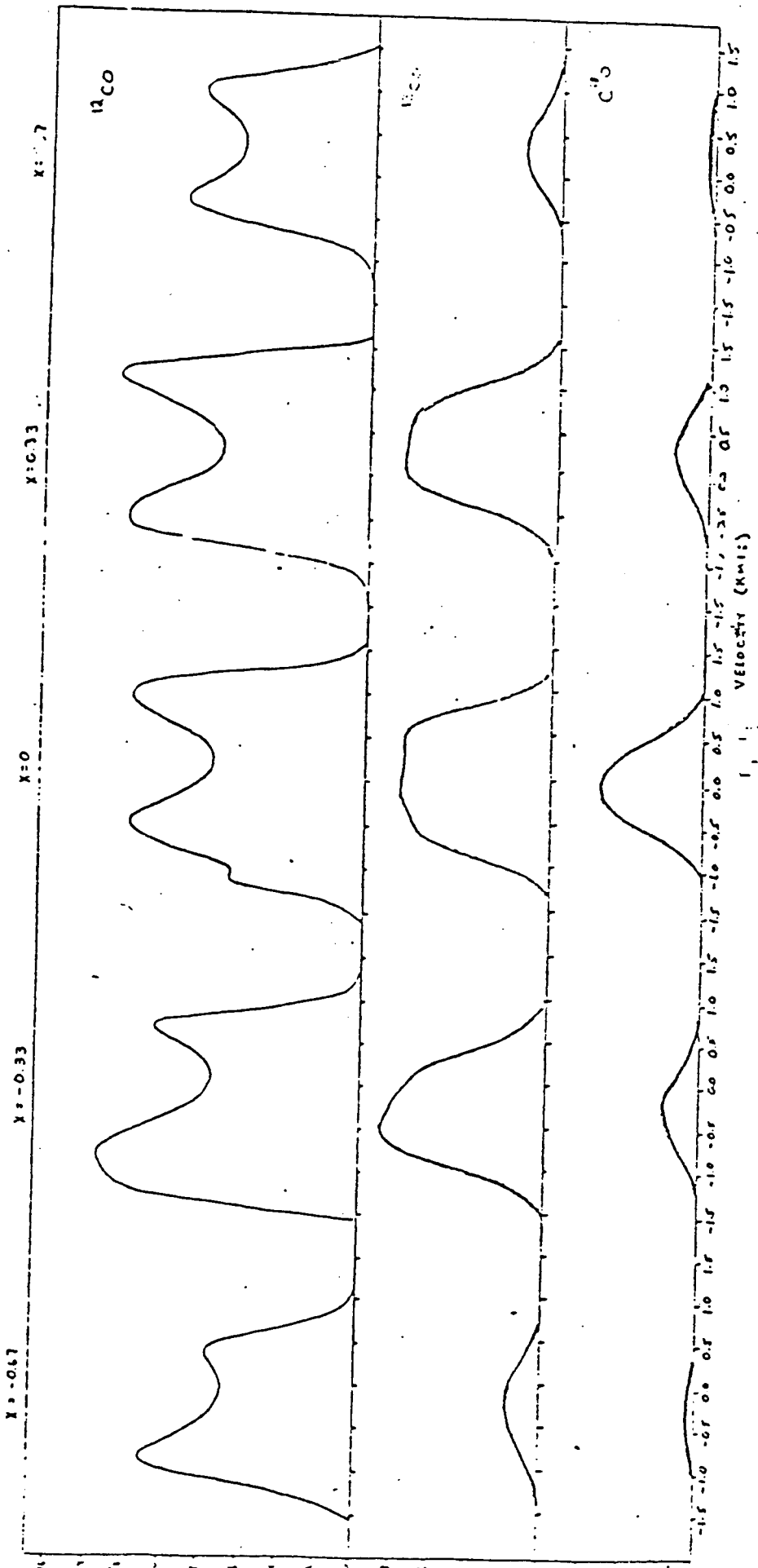


Figure 8

TMAX 1300 F21 N3

Maximum brightness temperature ( $^{\circ}\text{K}$ )

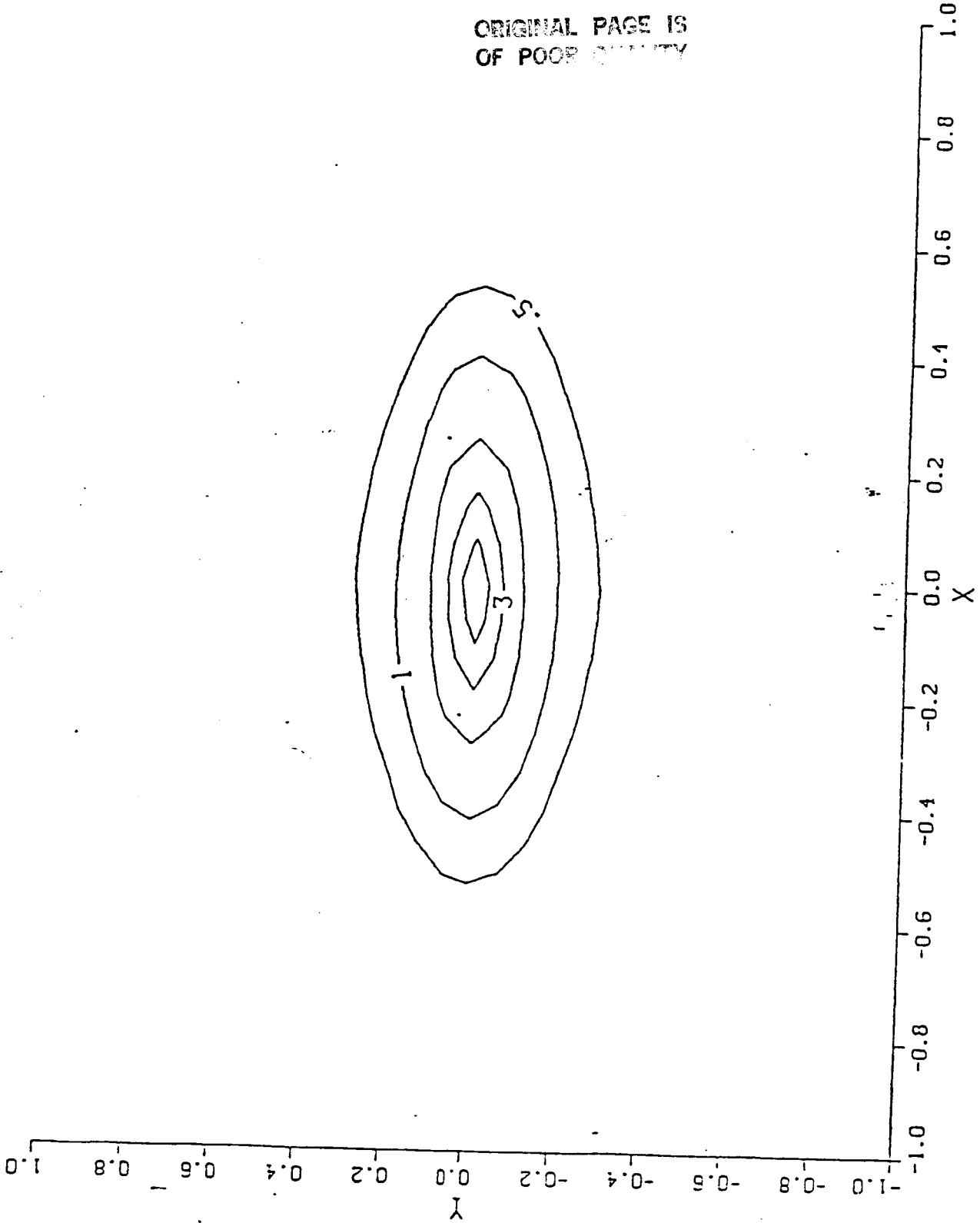


Figure 9a

FWHM 13CO F21 N3 Line width (km/sec)

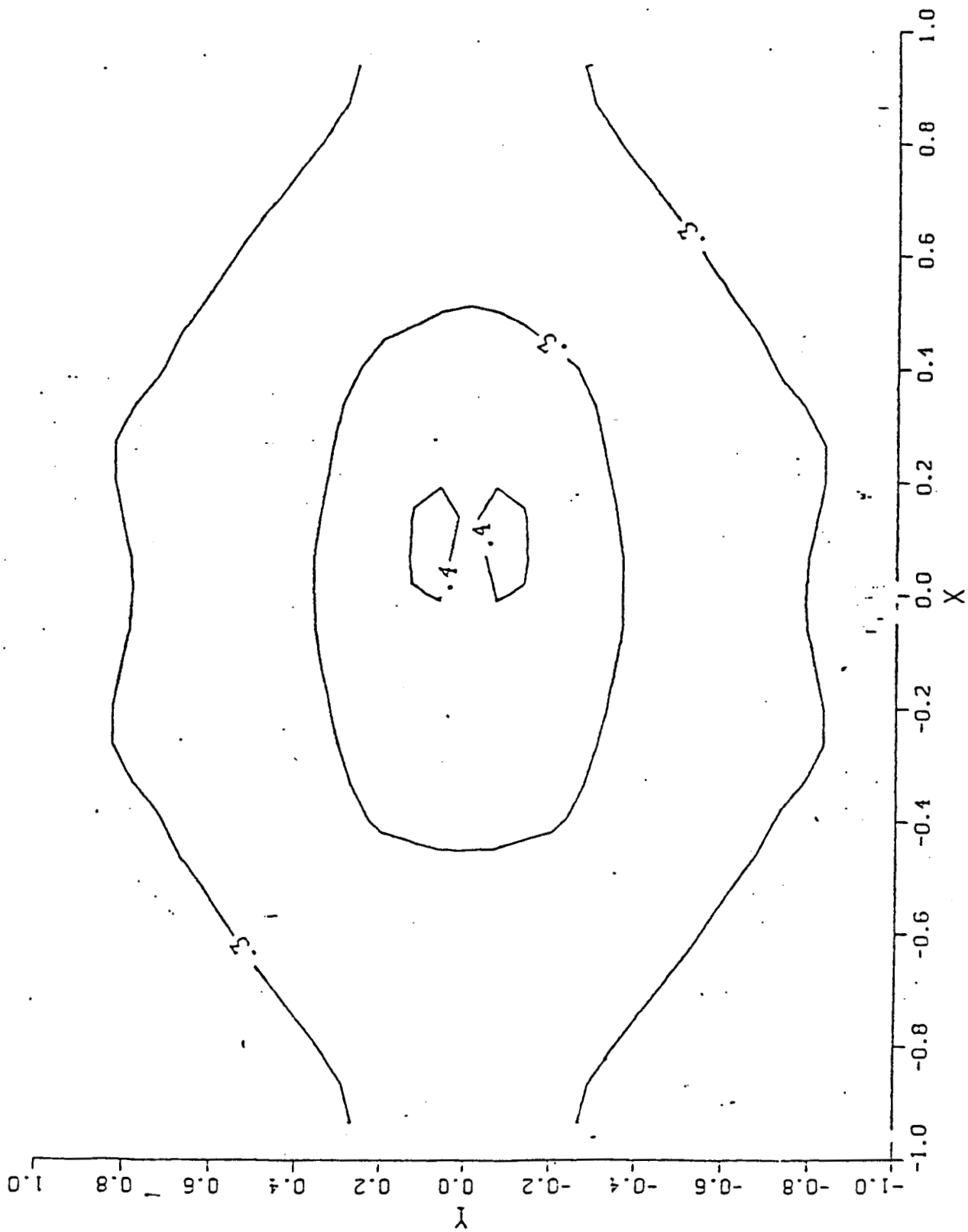


Figure 9b

VMEAN 13CO

F21 N3

Line Velocity (km/sec)

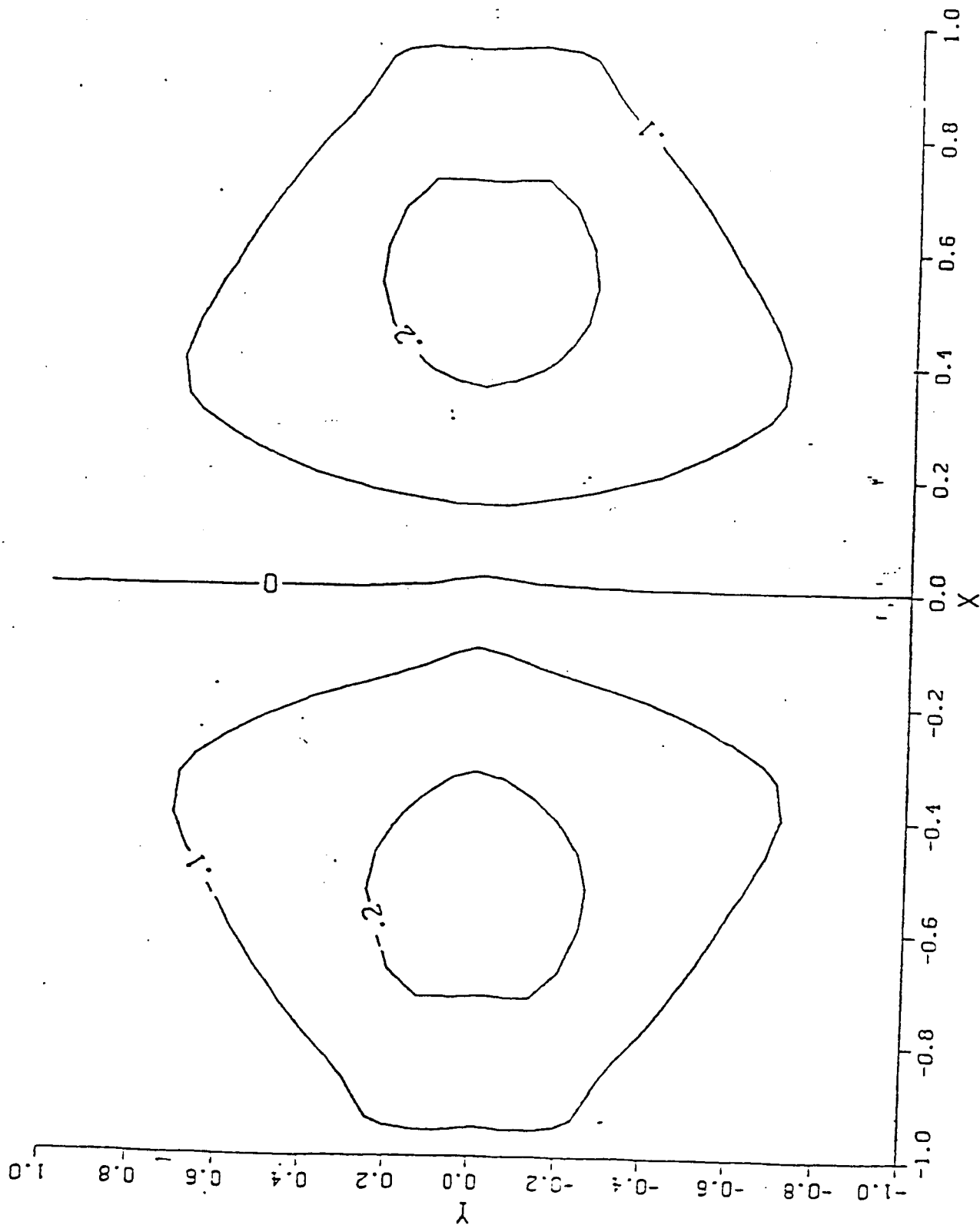


Figure 9c

Figure 10

